Heliyon 9 (2023) e14726

Contents lists available at ScienceDirect

Heliyon

journal homepage: www.cell.com/heliyon

Research article

Evaluation of optimal acquisition delays of DECT iodine maps in pancreatic adenocarcinoma: A potential alternative to the Patlak model of CT perfusion

Stephan Skornitzke, Philipp Mayer, Hans-Ulrich Kauczor, Wolfram Stiller *

Diagnostic and Interventional Radiology (DIR), Heidelberg University Hospital, Heidelberg, Germany

ARTICLE INFO

Keywords:
CT perfusion
Dual-energy CT
Iodine quantification
Pancreatic carcinoma

ABSTRACT

Introduction: By using bolus tracking with an appropriate acquisition delay dual-energy computed tomography (DECT) iodine maps might serve as a replacement of CT perfusion maps at reduced radiation exposure. This study aimed to evaluate the optimal acquisition delays of DECT for the replacement of parameter maps calculated with the Patlak model in pancreatic adenocarcinoma by corresponding iodine maps.

Materials and methods: Dual-source dynamic DECT acquisitions at 80 kV_p/Sn140 kV_p of 14 patients with pancreatic carcinoma were used to calculate CT perfusion maps of blood volume and permeability with the Patlak model. DECT iodine maps were generated from individual DECT acquisitions, matching acquisition times relative to prior bolus-triggered three-phase CT acquisitions for investigating different acquisition delays. Correlation between perfusion parameters and iodine concentrations was determined for acquisition delays between −6 s and 33 s.

Results: Correlation between iodine concentrations and perfusion parameters ranged from −0.05 to 0.63 for blood volume and from −0.05 to 0.71 for permeability, depending on potential trigger delay. The correlation was significant for potential acquisition delays above 1.5 s for blood volume and above 9.0 s for permeability (both $p < 0.05$). Maximum correlation occurred at an acquisition delay of 15.0 s for blood volume ($r = 0.63$) and at 25.5 s for permeability ($r = 0.71$), with significantly lower iodine concentrations in carcinoma (15.0 s: 1.3 ± 0.5 mg/ml; 22.5 s: 1.4 ± 0.7 mg/ml) than in non-neoplastic pancreatic parenchyma (15.0 s: 2.3 ± 0.8 mg/ml; 22.5 s: 2.4 ± 0.6 mg/ml; $p < 0.05$).

Discussion: In the future, well-timed DECT iodine maps acquired with bolus tracking could provide an alternative to permeability and blood volume maps calculated with the Patlak model.

1. Introduction

Dual-energy computed tomography (DECT) is a technique that relies on the acquisition of computed tomography (CT) image data at two different mean photon energy levels. As the physical mechanisms of x-ray absorption are dependent on the photon energy, the complementary information from the two datasets allows for a large number of post-processing applications [1–5]. In particular,

* Corresponding author. Diagnostic and Interventional Radiology (DIR) Heidelberg University Hospital Im Neuenheimer Feld 130.3 69120 Heidelberg, Germany

E-mail addresses: stephan.skornitzke@med.uni-heidelberg.de (S. Skornitzke), philipp.mayer@med.uni-heidelberg.de (P. Mayer), hans-ulrich.kauczor@med.uni-heidelberg.de (H.-U. Kauczor), wolfram.stiller@med.uni-heidelberg.de (W. Stiller).

https://doi.org/10.1016/j.heliyon.2023.e14726
Received 3 June 2022; Received in revised form 24 February 2023; Accepted 15 March 2023
Available online 22 March 2023

quantitative DECT iodine maps based on three-material decomposition have been of interest for the evaluation of abdominal tumors. Based on the fact that tumor angiogenesis strongly influences contrast agent distribution, which can be quantified by DECT iodine concentration measurements, iodine maps have been applied for the diagnosis of abdominal tumors, e.g. allowing for differentiation of tumor types [1,6,7]. Furthermore, studies have evaluated the use of DECT iodine maps in therapy response assessment, investigating the effectiveness of chemotherapy treatment in pancreatic carcinoma and hepatocellular carcinoma [3,8].

Despite its relatively low incidence, pancreatic carcinoma remains one of the most common causes of cancer mortality [9]. While surgery improves survival, it is considered feasible only in a limited number of patients and re-occurrence is common [9,10]. This makes pancreatic carcinoma an important target for the development and application of quantitative imaging biomarkers to improve diagnosis and treatment response assessment [3,10].

Expanding on the idea of using DECT iodine maps to visualize angiogenesis, there have also been attempts to establish single-acquisition DECT iodine maps as a quantitative imaging biomarker for tissue perfusion. Possibly, DECT iodine maps could provide a dose-reduced alternative to CT perfusion, which is the current gold standard for quantitative measurements of tissue perfusion in CT [11,12]. To this end, several studies have tried to elucidate the connection between measured iodine concentrations and perfusion parameters by correlating the DECT iodine maps to quantitative maps of tissue perfusion obtained from dynamic CT perfusion acquisitions. Initially, Zhang et al. showed a significant correlation between measured iodine concentrations and parameters of liver perfusion in rabbits with VX2 liver tumors [13]. Stiller et al. translated the approach to the human pancreas, reporting on the dependence of the correlation between measured iodine concentrations and blood flow on the acquisition time of the DECT iodine maps [14]. Further research by Thaiss et al. and Mulé et al. provided similar results for hepatocellular carcinoma and lymphoma [15,16]. However, these previous studies were limited in their evaluation of potential optimum acquisition timings and could not yet provide a clinically feasible method for acquisition of suitable DECT iodine maps. Therefore, Gordic et al. and Skornitzke et al. each determined an optimum acquisition time for bolus tracking-triggered DECT acquisition to achieve maximum correlation [17,18]. Nonetheless, results from Skornitzke et al. remain limited to the perfusion parameter blood flow derived using the Maximum-slope model of Miles, while Gordic et al. focused on the liver only, where liver-specific perfusion models are used.

The main hypothesis of this study was that DECT iodine maps of the pancreas might be a suitable replacement of CT perfusion measurements with the Patlak model, i.e. for the determination of the parameters blood volume and permeability surface-area product, which, to date, has not been evaluated. In this study, correlation between quantitative DECT iodine concentration measurements and these two CT-perfusion parameters was quantitatively assessed in a patient collective. Iodine concentrations at the time of maximum correlation were evaluated for their diagnostic use. In the future, this approach would allow the acquisition of well-timed DECT iodine maps that could be used as quantitative imaging biomarkers for the functional assessment of tissue perfusion, aiming to improve oncologic imaging of pancreatic carcinoma.

2. Material and methods

2.1. Patient collective

This study was performed in accordance with the standards set by the World Medical Association (Declaration of Helsinki 2013) and with approval from the local Ethics Committee of the Medical Faculty Heidelberg. Prospective data acquisition was performed as part of a previously published study [18]. All patients consented to the prospective data acquisition. Main inclusion criterion was the strong clinical suspicion of pancreatic adenocarcinoma based on previous clinical examinations (CT, MRI, ultrasound) [18]. Exclusion criteria were previous treatment for pancreatic carcinoma, final histopathological diagnosis other than pancreatic carcinoma (n = 3), conditions prohibiting contrast-enhanced CT (decreased kidney function, manifested hyperthyroidism, allergy or sensitivity to iodinated contrast agent), denial of consent, prolonged time difference between CT acquisitions (not performed within one session; n = 3), and inability to reproduce the shallowing breathing technique for perfusion CT (n = 2). In total, 22 patients could be included for data acquisition, of which 14 patients could be included in this analysis. See Table 1 for an overview of inclusion and exclusion criteria and Table 2 for an overview of clinical and pathological patient characteristics.

Table 1
Overview of inclusion and exclusion criteria for this study.

Inclusion criteria	n = 22
Strong clinical suspicion of pancreatic adenocarcinoma	
Informed consent to prospective data acquisition	
Exclusion criteria	**Σn = 8**
Final histopathological diagnosis other than pancreatic carcinoma	n = 3
Pancreatitis	n = 1
Pancreatic neuroendocrine tumor	n = 1
Dedifferentiated tumor	n = 1
Conditions prohibiting contrast-enhanced CT (decreased kidney function, manifested hyperthyroidism, allergy, or sensitivity to iodinated contrast agent)	n = 0
Denial of consent	n = 0
Prolonged time difference between CT acquisitions (not performed within one session)	n = 3
Inability to reproduce shallow breathing technique for perfusion CT	n = 2
Final number of patients	**n = 14**

Table 2
Overview of clinical and pathological patient characteristics.

Median Age (interquartile range, IQR)	62.5 years (59–69 years)
Sex	
Female	8 (57.1%)
Male	6 (42.9%)
Histopathological diagnosis	
PDAC	14 (100.0%)
Other	0 (0.0%)
Median tumor size (IQR)	**3.6 cm (2.6–4.5 cm)**
T stage	
T1	0 (0.0%)
T2	8 (57.1%)
T3	4 (28.6%)
T4	1 (7.1%)
not available	1 (7.1%)
N stage	
N0	4 (28.6%)
N1	3 (21.4%)
N2	5 (35.7%)
not available	2 (14.3%)
M stage	
M0/MX	13 (92.9%)
M1	1 (7.1%; peritoneal metastases)
Grading	
G1	0 (0.0%)
G2	9 (64.3%)
G3	3 (21.4%)
not available	2 (14.3%)
Tumor location	
Pancreatic head	11 (78.6%)
Pancreatic body and/or tail	3 (21.4%)
Type of surgery	
ppWhipple	4 (28.6%)
cWhipple	1 (7.1%)
Left resection	2 (14.3%)
Total pancreatectomy	5 (35.7%)
Diagnostic laparotomy[a]	2 (14.3%)

Abbreviations: cWhipple, conventional Whipple procedure; IQR, interquartile range; PDAC, pancreatic ductal adenocarcinoma; ppWhipple, pylorus-preserving Whipple procedure.

[a] Tumor resection was not indicated in one patient with intraoperatively detected peritoneal metastases and not possible in one patient with tumor invasion of the superior mesenteric artery.

2.2. CT imaging protocol

For tumor localization and clinical diagnosis, patients were first examined with a routine protocol for three-phase contrast-enhanced abdominal CT on a dual-source DECT scanner (SOMATOM Definition Flash, Siemens Healthineers; Erlangen, Germany). Acquisitions were performed in hydro-CT technique after the injection of 80 ml of iodinated contrast agent (370 mg/ml iodine concentration) at a flow rate of 5 ml/s [19]. The arterial and venous phase CT acquisitions were started by a bolus trigger with a delay of 10 s and 40 s, respectively, after the CT numbers measured in the abdominal aorta at the level of the coeliac trunk exceeded the trigger threshold of 120 HU. All three phases were acquired with automated exposure control (CARE kV and CARE Dose 4D, Siemens Healthineers; Erlangen, Germany) with a reference tube potential of 120 kV_p and a reference tube current-time product of 210 mAs. The pitch was set to 0.6 and collimation was 64 × 0.6 mm. Average scan coverage was 26.1 cm for native phase acquisitions, 26.0 cm for arterial phase acquisitions, and 46.9 cm for venous phase acquisitions.

After a 15-minute break to allow for clearance of contrast agent, patients were then examined with a dynamic DECT perfusion protocol, where each individual acquisition was performed in dual-energy mode. Following contrast agent injection (80 ml, with additional 40 ml saline solution chaser), the dynamic acquisition was started after a fixed delay of 13 s. The dynamic acquisition itself consisted of 34 DECT acquisitions without patient table feed, performed in 1.5 s intervals, spanning a total time of 51 s. Each DECT acquisition was performed with tube potentials of 80 kV_p and Sn140 kV_p (i.e. with tin filtration) and with automated tube current modulation (reference values: 270 mAs and 104 mAs, respectively). Collimation was 32 × 0.6 mm. Scan coverage for dynamic DECT acquisitions was 1.92 cm (no table feed). Images were reconstructed with a soft-tissue kernel (B30f) and a slice thickness/increment of 0.6 mm for post-processing and 5 mm for segmentation, respectively, as described in detail below.

Table 3
Overview of the patient radiation exposure corresponding to the conventional three-phased contrast-enhanced abdominal CT, the individual DECT acquisition at the proposed time points and the dynamic CT-perfusion acquisition at 80kV$_p$, encompassing all of the 34 acquisitions. Note the slight differences between individual DECT acquisitions caused by the tube-current modulation.

	CTDI$_{vol}$ [mGy]	DLP [mGy·cm]	D$_{eff}$ [mSv]	%Dose compared to 80 kV$_p$ CT-perfusion
Native phase	6.40 ± 1.28	168.61 ± 45.32	2.58 ± 0.69	N/A
Arterial phase	5.13 ± 1.07	134.05 ± 35.51	2.05 ± 0.54	N/A
Venous phase	5.28 ± 1.00	249.91 ± 61.15	3.82 ± 0.94	N/A
DECT acquisition at t = 15.0 s corresponding to blood volume	6.55 ± 1.53	12.58 ± 29.30	0.19 ± 0.04	4.86%
DECT acquisition at t = 25.5 s corresponding to permeability	6.54 ± 1.52	12.57 ± 29.30	0.19 ± 0.04	4.85%
DECT acquisition at t = 19.5 s corresponding to blood flow	6.54 ± 1.53	12.57 ± 26.40	0.19 ± 0.05	4.85%
Dynamic CT-perfusion acquisition at 80kV$_p$	134.82 ± 36.25	258.84 ± 69.60	3.96 ± 0.20	100%

Patient radiation exposure was recorded in terms of volumetric CT dose index (CTDI$_{vol}$) and dose-length product (DLP) for all of the acquisitions. Recorded CTDI$_{vol}$ and DLP, as well as calculated effective Dose (D$_{eff}$), are given in Table 3.

2.3. Post-processing

As the basis for the post-processing, data was segmented by an experienced radiologist (4 years of experience in abdominal radiology), who was not blinded to the histopathologically confirmed diagnosis. For the segmentation, one 5 mm reference slice was selected from the dynamic DECT acquisition for each patient, on which the outline of the pancreas was drawn to determine the evaluation region. Furthermore, circular regions of interest (ROI) were placed in non-neoplastic pancreatic tissue and pancreatic carcinoma for evaluation of DECT iodine maps and perfusion maps using software developed in-house [14]. These ROIs were placed on the reference slice of the original 80 kV$_p$ images and later copied to the exact same location in the DECT iodine maps and perfusion maps. ROIs were drawn as large as possible inside their respective tissue types.

A deformable motion-correction was applied to the 80 kV$_p$ image data of the dynamic acquisition, registering each time step to the selected reference slice [20]. Acquisitions that could not be registered to the selected reference slice were excluded from the evaluation. Results of the motion correction were also applied to the intrinsically co-registered Sn140 kV$_p$ image data.

DECT iodine maps were calculated from the motion-corrected image data for each individual DECT acquisition, i.e. up to 34 iodine maps were calculated for each patient [18]. Iodine maps were calculated based on three-material decomposition with an algorithm implemented in software developed in-house [14]. For time points excluded during motion correction, data from the previous acquisition was used instead. If the excluded time point was the first acquisition, data from the second acquisition was used instead.

Perfusion maps of permeability surface-area product (or permeability for short) and blood volume were calculated from the 80 kV$_p$ image data with the Patlak model, based on an implementation in software developed in-house [21].

2.4. Evaluation

While the dynamic DECT acquisition was started with a fixed delay of 13 s after contrast agent injection, the data from the previous three-phase contrast-enhanced abdominal CT acquisition, which was acquired with bolus tracking, was used to evaluate a potential DECT acquisition using bolus tracking by using a previously described technique called “simulated bolus tracking” [18]. Based on the data from the previous three-phase acquisition, the actual timing of the bolus trigger (i.e. the “bolus trigger time”) was calculated from the time difference between the start of the injection of the contrast agent and the start of the arterial phase image acquisition for each patient. Relying on the assumption that the patients’ circulatory function did not change significantly during the 15 minute break for contrast agent clearance, the bolus trigger time can then be put in relation to the acquisition timing of the dynamic DECT acquisition in the same patient. Thus, each of the individual DECT acquisitions of the complete dynamic DECT series corresponds to a unique value for the “trigger delay”, which is used to trigger CT acquisitions after the CT-number threshold for bolus tracking is reached (e.g. the delay of 10 s or 40 s for the arterial and venous phase acquisition). Calculated “trigger delays” were rounded down to the next multiple of 1.5 s and only values where data was available for all patients were included, to facilitate comparison between patients. As the dynamic CT-perfusion acquisition was started before contrast agent arrived in the abdominal aorta, where attenuation would usually be measured for the bolus trigger, the minimum potential trigger delay was −6 s, i.e. 6 s before the trigger threshold of 120 HU would have been reached for an arterial phase acquisition. The maximum potential trigger delay was 33 s [18].

For quantitative comparison, the iodine concentrations measured in an ROI in non-neoplastic pancreatic tissue and carcinoma were correlated to the calculated perfusion parameters of the Patlak model, calculating Pearson’s correlation coefficient for each trigger delay. Student’s t-test was used to test for differences between non-neoplastic pancreatic tissue and carcinoma in Patlak perfusion parameters as well as in DECT iodine concentrations at the time points of maximum correlation. Additionally, linear regression was performed to estimate perfusion parameters from DECT iodine concentrations at the time of maximum correlation, calculating average and maximum relative errors. The significance threshold for p-values was set at $p < 0.05$. Image analysis was performed using software developed in-house, while EXCEL 2016 (Microsoft, Redmond, United States) was used for statistical analysis [14].

Additionally, earlier results from the previous study were used for comparison, namely, the quantitative measurement of iodine concentrations in non-neoplastic pancreatic tissue and carcinoma, the measurement of blood flow, as calculated with the Maximum-slope model, and the correlation between the iodine concentrations and blood flow [18].

3. Results

Motion correction could be performed successfully in all 14 patients. DECT iodine maps could be derived and perfusion maps of blood volume and permeability could be calculated using the Patlak model for all patients, see Fig. 1 (A - F). Bolus trigger times could be determined for all patients, based on which simulated bolus tracking could be performed. A total of 27 acquisitions could be matched, allowing to evaluate trigger delays between −6 s (i.e. before the trigger threshold is exceeded) and 33 s.

3.1. Patlak perfusion parameters

On average, blood volume was 5.9 ± 3.0 ml/100 ml in pancreatic carcinoma and 18.5 ± 13.1 ml/100 ml in non-neoplastic pancreatic tissue, respectively (see Fig. 2 (A)). The difference in blood volume between tissue types was statistically significant ($p < 0.05$). For permeability, the average value in pancreatic carcinoma was 20.9 ± 12.2 ml/100 ml/min and the average value in non-neoplastic pancreatic tissue was 31.2 ± 16.8 ml/100 ml/min (cf. Fig. 2 (B)). The difference in permeability between tissue types was also statistically significant ($p < 0.05$). Results are summarized in Table 4.

3.2. DECT iodine concentrations

The correlation between measured perfusion parameters and iodine concentrations showed a strong dependence on the acquisition time of the DECT iodine map (see Table 5). When considering both tissue types, correlation with iodine concentrations was higher for measurements of permeability (maximum $r = 0.71$) than for measurements of blood volume (maximum $r = 0.63$). For comparison, maximum correlation for blood flow was $r = 0.89$ [18]. For blood volume, the maximum in correlation occurred at 15.0 s after simulated bolus trigger, at which point the average iodine concentration was 1.3 ± 0.5 mg/ml in pancreatic carcinoma and 2.3 ± 0.8 mg/ml in non-neoplastic pancreatic parenchyma, see Fig. 3 (A). The maximum for permeability occurred at 25.5 s, with iodine concentrations of 1.4 ± 0.7 mg/ml in pancreatic carcinoma and 2.4 ± 0.6 mg/ml in non-neoplastic pancreatic parenchyma (cf. Fig. 3 (B)) and at 19.5 s for blood flow, with iodine concentrations of 1.4 ± 0.6 mg/ml in pancreatic carcinoma and 2.4 ± 0.8 mg/ml in non-neoplastic pancreatic parenchyma (cf. Fig. 3 (C)) [18]. Examples of perfusion maps and the respective DECT iodine map

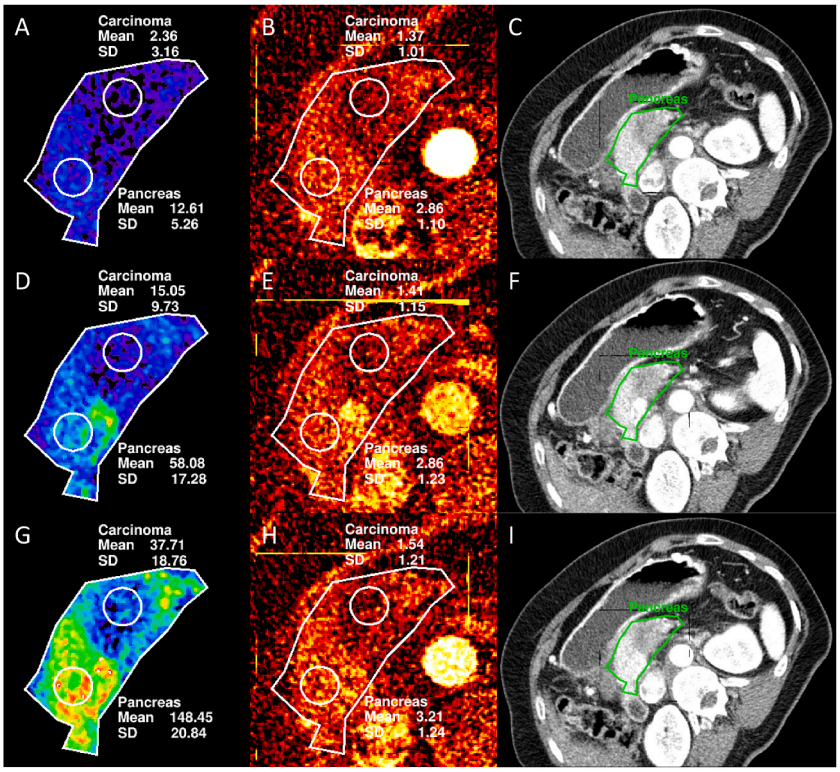

Fig. 1. Image examples for quantitative perfusion maps calculated with the Patlak model and the Maximum-slope model (results previously published and given for comparison) [18] compared to the quantitative iodine map corresponding to the trigger delay with the highest correlation (see also Table 5) and a conventional 80 kV_p image acquired at the same time as the iodine map. Blood volume map (A), iodine map (B), and conventional image (C) at t = 15.0 s. Permeability map (D), iodine map (E), and conventional image (F) at t = 25.5 s. Blood flow map (G), iodine map (H), and conventional image (I) at t = 19.5 s.

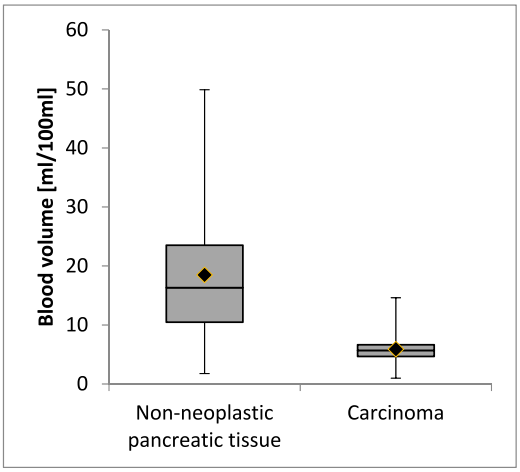

(a)

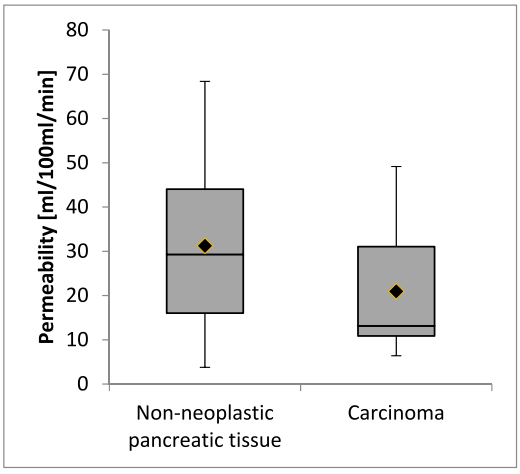

(b)

Fig. 2. Boxplots (median, quartiles, minimum and maximum values) of the measurements of blood volume (A) and permeability (B) with the Patlak model in non-neoplastic pancreatic tissue and carcinoma.

Table 4
Summary of the evaluation of perfusion maps calculated with the Patlak model and the Maximum-slope model in non-neoplastic pancreatic tissue and pancreatic carcinoma. Note that a statistically significant difference between tissue types was observed for all perfusion parameters. Results from the Maximum-slope model are given for comparison [18].

	Blood volume (Patlak) [ml/100 ml]	Permeability (Patlak) [ml/100 ml/min]	Blood flow (Maximum-slope) [ml/100 ml/min]
Non-neoplastic pancreatic tissue	18.5 ± 13.1	31.2 ± 16.8	87.6 ± 28.4
Carcinoma	5.9 ± 3.0	20.9 ± 12.2	38.6 ± 22.2
p-value of *t*-test	0.0009	0.018	<0.0001

corresponding to the delay with the highest correlation are shown in Fig. 1 (A - I), while descriptive statistics of iodine concentrations measured at the time of maximum correlation are shown in Fig. 3 (A - C) and Table 6. For all three parameters, an influence of tissue type on the correlation was observed. Correlation between perfusion parameters and iodine concentrations was higher in pancreatic carcinoma than in non-neoplastic pancreatic tissue, with permeability showing the largest differences. Regression equations to estimate blood volume, permeability, and blood flow from iodine concentrations measured at the time of maximum correlation are also given in Table 6.

Table 5
Correlation coefficients between measured perfusion parameters (permeability, blood volume, blood flow) to the iodine concentrations measured for each evaluated time point, by tissue type. The last row shows the maximum correlation coefficient for each category. Correlation coefficients corresponding to a p-value of $p < 0.05$ are highlighted in bold print. Note the difference in sample size when evaluating individual tissue types ($n = 14$) and pooling tissue types ($n = 28$) leading to differences in significance thresholds.

	Blood volume			Permeability			Blood flow		
Time since bolus trigger [s]	All	Non-neoplastic pancreatic tissue	Carcinoma	All	Non-neoplastic pancreatic tissue	Carcinoma	All	Non-neoplastic pancreatic tissue	Carcinoma
−6.0	0.06	−0.05	**0.57**	0.27	0.24	0.37	0.22	0.23	0.43
−4.5	−0.05	−0.10	0.29	0.17	−0.05	**0.59**	−0.03	−0.27	0.41
−3.0	0.36	**0.60**	0.38	0.07	−0.29	0.46	0.22	0.22	0.40
−1.5	−0.05	0.02	0.39	0.14	−0.08	0.53	0.12	0.19	**0.55**
0.0	0.14	0.33	0.49	−0.05	−0.25	0.43	0.03	0.04	**0.53**
1.5	0.31	0.20	0.39	0.26	−0.10	**0.56**	**0.49**	0.49	0.40
3.0	**0.39**	0.29	0.28	0.25	0.00	0.48	**0.54**	0.50	0.43
4.5	**0.51**	0.49	0.39	0.12	−0.21	**0.65**	**0.49**	0.41	**0.56**
6.0	**0.58**	0.48	0.35	0.24	−0.18	**0.58**	**0.77**	**0.82**	0.49
7.5	**0.51**	0.41	0.29	0.30	−0.10	**0.78**	**0.62**	0.49	**0.61**
9.0	**0.61**	0.52	0.21	0.20	−0.16	**0.57**	**0.71**	**0.66**	**0.54**
10.5	**0.61**	0.46	0.36	**0.39**	−0.06	**0.76**	**0.81**	**0.72**	**0.63**
12.0	**0.60**	0.52	0.07	**0.39**	0.00	**0.82**	**0.79**	**0.75**	**0.62**
13.5	**0.61**	0.45	**0.59**	**0.43**	0.10	**0.65**	**0.77**	**0.65**	**0.65**
15.0	**0.63**	0.52	0.17	**0.39**	−0.04	**0.84**	**0.78**	**0.65**	**0.68**
16.5	**0.59**	0.37	0.46	**0.45**	0.14	**0.71**	**0.82**	**0.71**	**0.66**
18.0	**0.62**	0.46	**0.57**	**0.53**	0.09	**0.85**	**0.84**	**0.64**	**0.82**
19.5	**0.53**	0.31	0.46	**0.51**	0.18	**0.76**	**0.89**	**0.88**	**0.80**
21.0	**0.57**	0.38	**0.64**	**0.60**	0.31	**0.82**	**0.82**	**0.61**	**0.86**
22.5	**0.47**	0.32	0.28	**0.44**	0.07	**0.75**	**0.72**	**0.64**	**0.60**
24.0	**0.52**	0.33	0.50	**0.56**	0.25	**0.87**	**0.74**	0.51	**0.80**
25.5	**0.48**	0.14	0.51	**0.71**	**0.55**	**0.84**	**0.85**	**0.68**	**0.82**
27.0	**0.46**	0.24	0.36	**0.58**	0.24	**0.83**	**0.76**	**0.63**	**0.67**
28.5	**0.56**	0.45	0.52	**0.60**	0.26	**0.80**	**0.78**	**0.61**	**0.76**
30.0	**0.39**	0.13	0.29	**0.67**	0.42	**0.85**	**0.69**	0.40	**0.72**
31.5	**0.46**	0.29	0.44	**0.63**	0.34	**0.85**	**0.67**	0.39	**0.72**
33.0	**0.43**	0.22	0.43	**0.69**	0.47	**0.87**	**0.74**	0.50	**0.79**
Max	**0.63**	**0.60**	**0.64**	**0.71**	**0.55**	**0.87**	**0.89**	**0.88**	**0.86**

3.3. Optimum acquisition time windows

Based on the measured correlation values stated above, an optimum time window for DECT acquisition triggered by bolus tracking can be proposed for achieving the highest potential correlation to the following perfusion parameters, as shown in Fig. 4.

- Blood volume (Patlak): 13.5–18.0 s delay
- Permeability (Patlak): 25.5–33.0 s delay
- Blood flow (Maximum-slope): 15.0–21.0 s delay [18].

The overlap in the proposed acquisition time windows for the blood flow and the blood volume can also be visualized by plotting the parameter values of each measurement against each other in a scatterplot, as shown in Fig. 5.

4. Discussion

The aim of this study was to evaluate the connection between DECT iodine maps and CT perfusion maps of permeability and blood volume, as calculated with the Patlak model. The results show that Patlak parameter maps of permeability and blood volume can be approximated by DECT iodine maps, if an appropriate acquisition time is chosen. The acquisition time corresponding to the highest correlation between the perfusion parameter and iodine concentrations depends on the perfusion parameter. Inversely, different perfusion parameters could be approximated by performing DECT acquisitions with different acquisition delays. Single DECT acquisition could thus be used to reduce patient radiation exposure by removing the need for a dynamic CT acquisition. When interpreting the proposed optimum acquisition time windows from a physiological point of view, the higher delay for the measurement of permeability can be explained by the fact that the extravasation into the tissue and extracellular space is an effect that happens on a larger time scale, especially compared to the blood flow, which, as assumed by the Maximum-slope model, can be determined from the first pass of the contrast agent bolus. At the same time, there is an overlap between the proposed acquisition times for blood volume and blood flow. From a theoretical point of view, this connection can be explained by the fact that, in indicator dilution theory, blood flow and blood volume are directly related by the mean transit time as follows [12]:

$$\text{Blood volume} = \text{blood flow} \bullet \text{mean transit time}$$

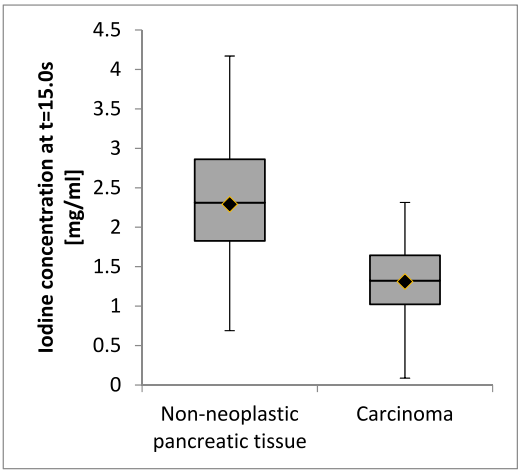

(a)

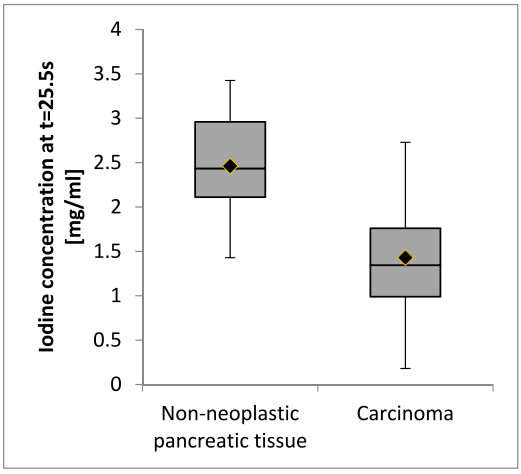

(b)

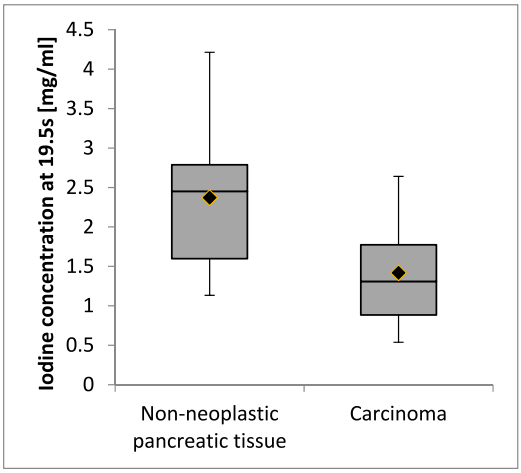

(c)

(caption on next page)

Fig. 3. Boxplots (median, quartiles, minimum and maximum values) of the measurements of iodine concentrations in non-neoplastic pancreatic tissue and carcinoma at the times of maximum correlation to the perfusion parameters blood volume (A), permeability (B), and blood flow (C).

Table 6
Iodine concentrations (IC) measured in non-neoplastic pancreatic tissue and carcinoma at the time when correlation to the respective perfusion parameter was at its maximum, maximum value of correlation and regression equation. Note the statistically significant difference between tissue types reported by Student's t-test.

	Iodine concentration corresponding to blood volume (t = 15.0 s) [mg/ml]	Iodine concentration corresponding to permeability (t = 25.5 s) [mg/ml]	Iodine concentration corresponding to blood flow (t = 19.5 s) [mg/ml]
Non-neoplastic pancreatic tissue	2.3 ± 0.8	2.4 ± 0.6	2.3 ± 0.8
Carcinoma	1.3 ± 0.5	1.4 ± 0.7	1.4 ± 0.6
p-value of *t*-test	0.0003	<0.0001	0.0001
Correlation	0.63	0.71	0.89
Regression equation	8.4 ml^2/100 ml/mg • IC - 2.8 ml/100 ml	13.5 ml^2/100 ml/mg/min • IC - 1.0 ml/100 ml/min	38.8 ml^2/100 ml/mg/min • IC - 11.6 ml/100 ml/min
Average %Error	91.4% (overall) 55.3% (pancreas) 127.5% (tumor)	31.9% (overall) 60.7% (pancreas) 3.1% (tumor)	14.4% (overall) −9.5% (pancreas) 38.3% (tumor)
Median %Error	4.5% (overall) −12.4% (pancreas) 48.0% (tumor)	4.4% (overall) 8.3% (pancreas) −5.4% (tumor)	−2.2% (overall) −9.0% (pancreas) 19.1% (tumor)
Maximum %Error	1307.2% (overall) 538.7% (pancreas) 1307.2% (tumor)	647.8% (overall) 647.8% (pancreas) −77.2% (tumor)	275.8% (overall) −47.0% (pancreas) 275.8% (tumor)

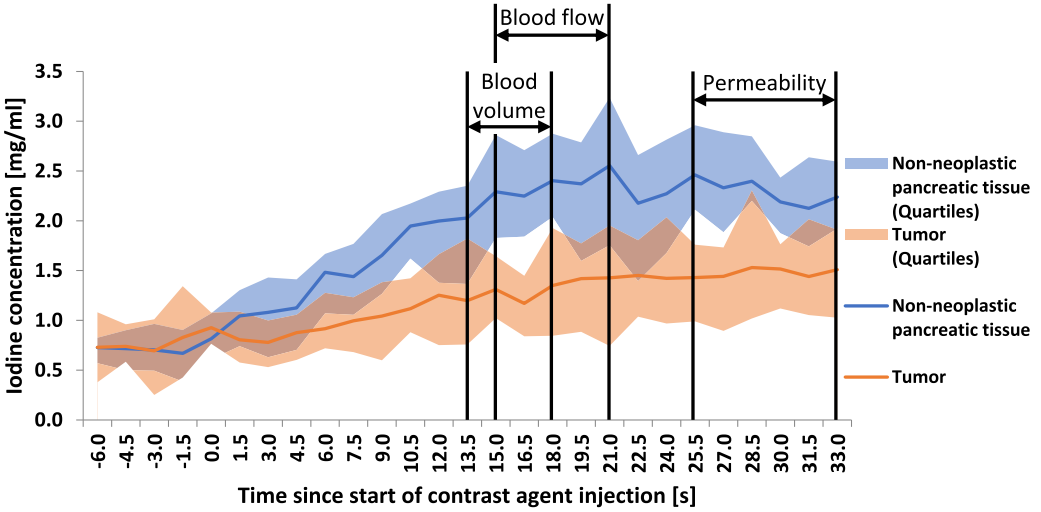

Fig. 4. Descriptive statistics (median, second and third quartile) of iodine concentrations over the corresponding trigger delay and suggested acquisition windows for blood volume, permeability, and blood flow (adapted from Skornitzke et al. with friendly permission from the British Journal of Radiology) [18].

Compared to the results obtained for the Maximum-slope model in the same patient collective in an earlier study, the maximum correlation is somewhat lower when evaluating the perfusion maps calculated with the Patlak model [18]. While this could mean that in general the parameter blood flow is easier to approximate with a single DECT acquisition, these differences could also be related to the input data and the underlying mathematical perfusion models. It has to be acknowledged that the acquisition protocol in this study was relatively short compared to other studies evaluating the Patlak model. For example, the 2012 guidelines for CT perfusion of the Experimental Cancer Medicine Centre Imaging Network Group recommend an acquisition duration of 60–90 s, compared to the 51 s used in this study [22].

Compared to other studies that did not use individually determined acquisition times, but relied on standard acquisition phases (i.e. native, arterial, and venous phase imaging) instead, the reported correlations in this study increased: Kang et al. reported correlations between 0.29 and 0.34 between iodine concentrations and blood flow, blood volume, and permeability in the human liver [23]. Zhang et al. observed stronger correlations for permeability in a rabbit VX2 liver tumors (up to 0.91), but lower correlations for blood volume (0.46) and blood flow (0.52) [13]. Studies with individually determined acquisition times achieved results on a similar order of

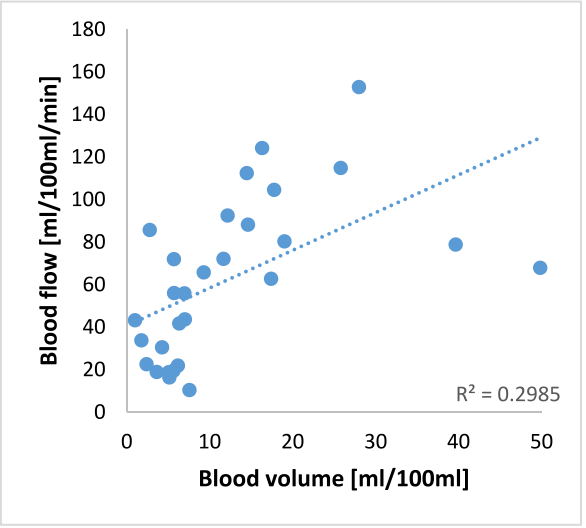

Fig. 5. Scatterplot of measured blood flow (Maximum-slope model) over measured blood volume (Patlak model) for each patient and linear regression illustrating the correlation between the two parameters.

magnitude to the results reported here [14,15,17]. However, Stiller et al. and Thaiss et al. did not suggest a suitable way to integrate their proposed DECT acquisition into clinical practice [14,15]. Gordic et al. achieved similar results to the current study, but results cannot be directly transferred from the liver to the pancreas because of the anatomical differences [17].

In the future, measurement of iodine concentrations at the proposed acquisition times could be compared to previously established values of perfusion parameters by linear regression, e.g. to compare results to previous studies. All calculated regression equations show an intercept close to 0 for all parameters, i.e. absence of iodine indicates absence of tissue perfusion. While the estimated relative error is quite high, the comparison of average error to median and maximum error indicates that there are outliers which could be caused by individual patient characteristics, insufficient image quality or insufficient motion-correction and might be corrected by additional pre- and post-processing.

Regarding the potential reduction in patient radiation exposure when replacing a dynamic CT perfusion acquisition with three individual well-timed DECT acquisitions, a dose-reduction of 85.4% could be achieved compared to conventional CT perfusion at 80 kV_p when using the same reference values for tube-current modulation as for the dynamic acquisitions. However, current contrast-enhanced three-phase abdominal CT acquisitions could also be adapted by adjusting acquisitions timings and replacing the native phase acquisition with virtual non-contrast images, to arrive at a three-phase abdominal DECT protocol. In that case, relinquishing the CT perfusion acquisition could lead to an overall dose-reduction of 30.5% compared to the combined three phases + dynamic acquisition at 80 kV_p, providing functional information on tissue perfusion with no increased dose compared to single-energy three-phase CT acquisitions. Furthermore, not all perfusion parameters might be necessary for the clinical task at hand and consequently less than three DECT acquisitions might be sufficient, e.g. if information on blood flow only is required.

Compared to conventional dynamic CT perfusion acquisitions, the proposed DECT acquisitions not only reduce patient radiation exposure but also require less post-processing. If DECT acquisitions were adapted for routine oncologic imaging, patients could benefit from the increased availability of DECT iodine maps as functional imaging biomarkers. This could improve early detection, treatment planning and therapy response assessment of cancer [3,10].

Regarding the limitations of this study, it has to be acknowledged that the overall acquisition time of the dynamic DECT perfusion protocol in this study was relatively short, as discussed above. Furthermore, the number of patients was limited, with only 14 patients that could be included in the evaluation. Therefore studies with a larger patient collective will have to confirm these findings in the future. However, the obtained results are generally in line with results observed in other studies. While previous studies have shown promising results for the liver, and while this study was able to investigate the pancreas, dedicated studies may be necessary for further organs to determine organ-specific acquisition times. Additionally, only one observer analyzed the images, precluding assessment of interobserver variability. Finally, prospective studies will be necessary to truly assess the potential of DECT iodine maps as an alternative to CT perfusion, determine clinically appropriate image quality and assess patient radiation exposure, and to evaluate the clinical use as an imaging biomarker in abdominal oncology.

In conclusion, the results show that the perfusion parameters permeability and blood volume, as calculated for the pancreas with the Patlak model, can be approximated by quantitative iodine concentration maps acquired from single DECT acquisitions, which could be triggered by bolus tracking using appropriate acquisition delays, respectively. The general approach of using DECT iodine maps to approximate perfusion parameters could be applied to different physiological models and perfusion parameters, as well as different abdominal organs. In the future, well-timed DECT acquisitions could be used to acquire specific quantitative imaging biomarkers individually selected for the clinical task at hand.

Author contribution statement

Wolfram Stiller: Conceived and designed the experiments; Analyzed and interpreted the data; Contributed reagents, materials, analysis tools or data; Wrote the paper.

Stephan Skornitzke: Conceived and designed the experiments; Performed the experiments; Analyzed and interpreted the data; Contributed reagents, materials, analysis tools or data; Wrote the paper.

Philipp Mayer: Performed the experiments; Contributed reagents, materials, analysis tools or data; Wrote the paper.

Hans-Ulrich Kauczor: Contributed reagents, materials, analysis tools or data; Wrote the paper.

Funding statement

This research did not receive any specific grant from funding agencies in the public, commercial, or not-for-profit sectors.

Data availability statement

The authors do not have permission to share data.

Declaration of interest's statement

The authors declare the following conflict of interests: Stephan Skornitzke has ownership interests in investment funds containing stock of healthcare companies. Wolfram Stiller is a member of the CT Advisory Board of Philips Medical Systems. Otherwise, the authors of this manuscript declare no relationships with any companies, whose products or services may be related to the subject matter of the article.

Acknowledgements

This research did not receive any specific grant from funding agencies in the public, commercial, or not-for-profit sectors.

Abbreviations

CT	computed tomography
$CTDI_{vol}$	volumetric computed tomography dose index
DECT	dual-energy computed tomography
DLP	dose-length product
D_{eff}	effective dose
IC	iodine concentration
MRI	magnetic resonance imaging
ROI	region-of-interest

References

[1] M.D. Agrawal, D.F. Pinho, N.M. Kulkarni, P.F. Hahn, A.R. Guimaraes, D.V. Sahani, Oncologic applications of dual-energy CT in the abdomen, Radiographics 34 (2014) 589–612, https://doi.org/10.1148/rg.343135041.

[2] K. Higashigaito, F. Angst, V.M. Runge, H. Alkadhi, O.F. Donati, Metal artifact reduction in pelvic computed tomography with hip prostheses: comparison of virtual monoenergetic extrapolations from dual-energy computed tomography and an iterative metal artifact reduction algorithm in a phantom study, Invest. Radiol. 50 (2015) 828–834, https://doi.org/10.1097/RLI.0000000000000191.

[3] S. Kawamoto, M.K. Fuld, D. Laheru, P. Huang, E.K. Fishman, Assessment of iodine uptake by pancreatic cancer following chemotherapy using dual-energy CT, Abdom Radiol 43 (2018) 445–456, https://doi.org/10.1007/s00261-017-1338-6.

[4] L. Beer, M. Toepker, A. Ba-Ssalamah, C. Schestak, A. Dutschke, M. Schindl, A. Wressnegger, H. Ringl, P. Apfaltrer, Objective and subjective comparison of virtual monoenergetic vs. polychromatic images in patients with pancreatic ductal adenocarcinoma, Eur. Radiol. 29 (2019) 3617–3625, https://doi.org/10.1007/s00330-019-06116-9.

[5] A. Kosmala, A.M. Weng, A. Heidemeier, B. Krauss, S. Knop, T.A. Bley, B. Petritsch, Multiple myeloma and dual-energy CT: diagnostic accuracy of virtual noncalcium technique for detection of bone marrow infiltration of the spine and pelvis, Radiology 286 (2017) 205–213, https://doi.org/10.1148/radiol.2017170281.

[6] A.M. Tawfik, A.A. Razek, J.M. Kerl, N.E. Nour-Eldin, R. Bauer, T.J. Vogl, Comparison of dual-energy CT-derived iodine content and iodine overlay of normal, inflammatory and metastatic squamous cell carcinoma cervical lymph nodes, Eur. Radiol. 24 (2014) 574–580, https://doi.org/10.1007/s00330-013-3035-3.

[7] B. Kaltenbach, J.L. Wichmann, S. Pfeifer, M.H. Albrecht, C. Booz, L. Lenga, R. Hammerstingl, T. D'Angelo, T.J. Vogl, S.S. Martin, Iodine quantification to distinguish hepatic neuroendocrine tumor metastasis from hepatocellular carcinoma at dual-source dual-energy liver CT, Eur. J. Radiol. 105 (2018) 20–24, https://doi.org/10.1016/j.ejrad.2018.05.019.

[8] T. Jiang, A. Kambadakone, N.M. Kulkarni, A.X. Zhu, D.V. Sahani, Monitoring response to antiangiogenic treatment and predicting outcomes in advanced hepatocellular carcinoma using image biomarkers, CT perfusion, tumor density, and tumor size (RECIST), Invest. Radiol. 47 (2012) 11–17, https://doi.org/10.1097/RLI.0b013e3182199bb5.

[9] S. Raimondi, P. Maisonneuve, A.B. Lowenfels, Epidemiology of pancreatic cancer: an overview, Nat. Rev. Gastroenterol. Hepatol. 6 (2009) 699–708.

[10] F. Fritz, S. Skornitzke, T. Hackert, H.U. Kauczor, W. Stiller, L. Grenacher, M. Klauss, Dual-energy perfusion-CT in recurrent pancreatic cancer – preliminary results, Rofo Fortschr Geb Rontgenstr Neuen Bildgeb Verfahr 188 (2016) 559–565, https://doi.org/10.1055/s-0042-105765.
[11] S.H. Kim, A. Kamaya, J.K. Willmann, CT perfusion of the liver: principles and applications in oncology, Radiology 272 (2014) 322–344, https://doi.org/10.1148/radiol.14130091.
[12] K. Miles, Perfusion CT for the assessment of tumour vascularity: which protocol? Br. J. Radiol. 76 (2003) S36–S42, https://doi.org/10.1259/bjr/18486642.
[13] L.J. Zhang, S. Wu, M. Wang, L. Lu, B. Chen, L. Jin, J. Wang, A.C. Larson, G.M. Lu, Quantitative dual energy CT measurements in rabbit VX2 liver tumors: comparison to perfusion CT measurements and histopathological findings, Eur. J. Radiol. 81 (2012) 1766–1775, https://doi.org/10.1016/j.ejrad.2011.06.057.
[14] W. Stiller, S. Skornitzke, F. Fritz, M. Klauss, J. Hansen, G. Pahn, L. Grenacher, H.-U. Kauczor, Correlation of quantitative dual-energy computed tomography iodine maps and abdominal computed tomography perfusion measurements: are single-acquisition dual-energy computed tomography iodine maps more than a reduced-dose surrogate of conventional computed tomography perfusion? Invest. Radiol. 50 (2015) 703–708, https://doi.org/10.1097/RLI.0000000000000176.
[15] W.M. Thaiss, U. Haberland, S. Kaufmann, D. Spira, C. Thomas, K. Nikolaou, M. Horger, A.W. Sauter, Iodine concentration as a perfusion surrogate marker in oncology: further elucidation of the underlying mechanisms using Volume Perfusion CT with 80 kVp, Eur. Radiol. 26 (2016) 2929–2936, https://doi.org/10.1007/s00330-015-4154-9.
[16] S. Mulé, F. Pigneur, R. Quelever, A. Tenenhaus, L. Baranes, P. Richard, V. Tacher, E. Herin, H. Pasquier, M. Ronot, A. Rahmouni, V. Vilgrain, A. Luciani, Can dual-energy CT replace perfusion CT for the functional evaluation of advanced hepatocellular carcinoma? Eur. Radiol. 28 (2018) 1977–1985, https://doi.org/10.1007/s00330-017-5151-y.
[17] S. Gordic, G.D. Puippe, B. Krauss, E. Klotz, L. Desbiolles, M. Lesurtel, B. Müllhaupt, T. Pfammatter, H. Alkadhi, Correlation between dual-energy and perfusion CT in patients with hepatocellular carcinoma, Radiology 280 (2016) 78–87, https://doi.org/10.1148/radiol.2015151560.
[18] S. Skornitzke, F. Fritz, P. Mayer, M. Koell, J. Hansen, G. Pahn, T. Hackert, H.-U. Kauczor, W. Stiller, Dual-energy CT iodine maps as an alternative quantitative imaging biomarker to abdominal CT perfusion: determination of appropriate trigger delays for acquisition using bolus tracking, Br. J. Radiol. 91 (2018), 20170351, https://doi.org/10.1259/bjr.20170351.
[19] G. Richter, C. Wunsch, B. Schneider, M. Düx, E. Klar, R. Seelos, G. Kauffmann, Hydro-CT in the detection and staging of pancreatic carcinoma, Radiologe 38 (1998) 279–286, https://doi.org/10.1007/s001170050355.
[20] S. Skornitzke, F. Fritz, M. Klauss, G. Pahn, J. Hansen, J. Hirsch, L. Grenacher, H.U. Kauczor, W. Stiller, Qualitative and quantitative evaluation of rigid and deformable motion correction algorithms using dual-energy CT images in view of application to CT perfusion measurements in abdominal organs affected by breathing motion, Br. J. Radiol. 88 (2015), 20140683, https://doi.org/10.1259/bjr.20140683.
[21] C.S. Patlak, R.G. Blasberg, Graphical evaluation of blood-to-brain transfer constants from multiple-time uptake data. Generalizations, J. Cerebr. Blood Flow Metabol. 5 (1985) 584–590, https://doi.org/10.1038/jcbfm.1985.87.
[22] K. Miles, T.-Y. Lee, V. Goh, E. Klotz, C. Cuenod, S. Bisdas, A. Groves, M. Hayball, R. Alonzi, T. Brunner, Current status and guidelines for the assessment of tumour vascular support with dynamic contrast-enhanced computed tomography, Eur. Radiol. 22 (2012) 1430–1441, https://doi.org/10.1007/s00330-012-2379-4.
[23] H.-J. Kang, S.H. Kim, J.S. Bae, S.K. Jeon, J.K. Han, Can quantitative iodine parameters on DECT replace perfusion CT parameters in colorectal cancers? Eur. Radiol. 28 (2018) 4775–4782, https://doi.org/10.1007/s00330-018-5502-3.